Received: 18 March 2024 | Revised: 18 June 2024 | Accepted: 11 July 2024

DOI: 10.1002/pen.26882

RESEARCH ARTICLE

POLYMER ENGINEERING AND SCIENCE WILEY

Characterization, processing, and modeling of industrial recycled polyolefins

David O. Kazmer[1] | Sixtus O. Nzeh[1] | Beijun Shen[2] | David C. Elbert[2] | Ramaswamy Nagarajan[1] | Margaret Sobkowicz-Kline[1] | Thao D. Nguyen[2]

[1]Department of Plastics Engineering, University of Massachusetts Lowell, Lowell, Massachusetts, USA

[2]Department of Mechanical Engineering, Johns Hopkins University, Baltimore, Maryland, USA

Correspondence
Sixtus O. Nzeh, University of Massachusetts Lowell, Lowell, MA 01854, USA.
Email: sixtusdika@gmail.com

Abstract

This study aims to establish a systematic approach for characterizing recycled polyolefins of unknown composition, with a specific focus on predicting their performance in film extrusion. We explore various characterization techniques, including differential scanning calorimetry (DSC), Fourier-transform infrared spectroscopy (FTIR), thermogravimetric analysis (TGA), and rheometry to assess their effectiveness in identifying the polyethylene (PE) fractions within polypropylene (PP) recyclates. By integrating experimental data with modeling techniques, we aim to provide insights into the predictive capabilities of these techniques in determining processing behaviors. The research highlights the superior fidelity of DSC in predicting the relative fraction and type of PE in a PP recyclate. FTIR is also identified as a high-fidelity approach, albeit requiring application-specific calibration. TGA, capillary, and oscillatory rheometry are recognized for their ability to distinguish between grades of recycled polyolefins but provide aggregate behaviors rather than detailed constituent information. 3D flow simulation of the cast film extrusion investigated the effect of the viscosity characterization method, non-isothermal assumption, and process settings but could not fully replicate the observed variations in the cast film processing of two industrial polyolefins with similar melt flow rates and viscosity behaviors. This underscores the practical challenge of predicting processing issues prior to actual processing, necessitating reliance on reliable instrumentation suites and human expertise for diagnosing and remedying variations.

Highlights

- Two industrial recycled polypropylene materials having similar melt flow rates exhibit drastically different cast film processing behaviors.
- DSC and FTIR provide reasonable approaches for identifying constituent materials.
- Modeling of the melt viscosities characterized by capillary and parallel plate rheology suggests that viscosity variations relative to the power-law behavior

assumed in the coat hanger die design is a predominant driver of cast film instabilities.

KEYWORDS

film extrusion, flow simulation, materials characterization, plastic recycling, polyolefins

1 | INTRODUCTION

Polyolefins constitute about 55% of all plastics production with annual output currently exceeding 200 million metric tons.[1,2] Given continued economic growth, polyolefins production is expected to further double in the next 20 years.[3] Yet, only 5% of these plastics produced are recycled.[4] There are two primary barriers to increased recycling. First, there is the economic cost of recovery, as well as mechanical or chemical reprocessing which imparts both economic and technical challenges.[5,6] The primary technical challenge is the assurance of consistent and useful properties of the recycled material given variation in the recovered feedstocks. This research article investigates best practices in material characterization and modeling for recycled polyolefins and their blends. The work is part of the larger, Materials Genome Initiative (MGI) efforts to use data and data infrastructure to close the design loop and accelerate materials design.[7,8] Data supporting this contribution follow FAIR principles[9,10] and are available, along with MATLAB processing codes, at https://data.paradim.org/doi/k1mm-cf38/.

As recently reported by the Organization for Economic Cooperation and Development (OECD),[1] the proportion of production by polyolefin type shows that production is composed predominantly of 59% polyethylene (PE) and 39% polypropylene (PP) with slivers of ethylene-propylene-diene-monomer (EPDM), polyisobutylene (PIB), and others. The PE share is composed of around 49% high density (HDPE), 32% linear low density (LLDPE), 18% low density (LDPE), and less than 1% of ultra-high molecular weight (UHMWPE). Implied from the report is the challenge of materials identification and reuse. PE and PP have very similar properties as characterized in Table 1 for some 2677 grades from a widely used materials database.[11,12] (The number of specific polyolefin grades and production lots is orders of magnitudes greater as these 2677 grades are only those that are characterized and reported.) While "density is a key industrial parameter to identify the polymer type",[13] the densities for the various types of polyolefins are very similar such that they are not easily separable by cyclone[14] or sink–float[15] methods. The mechanical properties and vicat softening temperatures are greatest for PP followed by HDPE suggesting that these materials are of greater economic value as they enable less of a material to be used in more applications to meet end-use requirements. The melt flow rate (MFR) values, a measure of viscosity later discussed in more detail, have means on the same order of magnitude for injection molding grades while the extrusion grades of PE tend to have lower values typically representative of higher melt strength.

The fundamental issue in the reuse of polyolefins is that the recovered materials come from a variety of prior end-use applications. Generally, the best-case scenario is that a production run of the recovered materials comprises only one type of polyolefin (i.e., PP, HDPE, LDPE, or LLDPE) from a single application. Even in this case, however, the production practice is to characterize the melt flow of the recovered material per ASTM D1238 or ISO 1133 and then compound it with a lower or higher viscosity material using a rule of mixtures[16] to meet a target melt flow rate for resale (e.g., MFR of 5–10 or 20–30 g/10 min). More commonly, however, the recovered materials come from multiple applications and so are constituted of a variety of materials with different molecular weights and melt flow behaviors even if they comprised a single type of polyolefin. Even more commonly and worse, the recovered materials not only come from multiple applications but also comprised different types of polyolefins. In both of these latter two scenarios, the recovered materials are characterized and processed as if they are a single, homogeneous material. The result, however, is the dissemination of a polyolefin recyclate that is sold as recycled PE or PP but has a significant fraction of noncompliant materials. These recyclates may have melt densities and melt flow rates that meet purchasing specifications yet exhibit extremely different processing behaviors and resultant product performance. There is then a "network effect"[17] by which these materials propagate their variances to other recycled materials with continued reuse and recycling. Thus, there is a critical need for material characterization protocols by which material end-users and recyclers can identify the type of constitutive materials prior to use, recycling, and resale. In this study, we provide a practical assessment of material characterization methods for recycled polyolefins and a diagnosis of processing behaviors in two recycled polypropylenes.

TABLE 1 Property comparison of common types of polyolefins.

Molding grades	HDPE	LDPE	LLDPE	PP
Average density [g/cc]	0.954	0.921	0.924	0.930
Grade count	518	244	129	1137
Average tensile strength, yield [MPa]	26.2	11	14.9	31.7
Grade count	444	167	95	1121
Flexural modulus [GPa]	1.13	0.264	0.451	1.44
Grade count	395	128	80	1035
Average vicat softening point [°C]	120	89.7	96.3	122
Grade count	309	195	85	372
Average melt flow [g/10 min]	22.9	32.8	30.6	28.9
Grade count	503	222	126	1252
Extrusion grades	**HDPE**	**LDPE**	**LLDPE**	**PP**
Average density [g/cc]	0.958	0.921	0.928	0.916
Grade count	180	133	71	265
Average tensile strength, yield [MPa]	24.5	10.1	17.9	32.2
Grade count	116	25	30	245
Average flexural modulus [GPa]	1.20	0.199	0.481	1.40
Grade count	80	27	21	262
Average vicat softening point [°C]	116	91	107	136
Grade count	67	75	29	97
Average melt flow [g/10 min]	4.29	5.45	5.42	38.8
Grade count	179	119	72	315

1.1 | Methodology

A material characterization, processing, and modeling protocol is shown in Figure 1 as applied for two recycled polypropylenes; the protocol is modeled after industry practice and intended as a template for further development. As indicated in the left column, upon receipt of a material, processors will read the material safety data sheets (SDS), inspect the shape, color, odor, and density of the material, then test the melt flow rate. If the material conforms to specifications, then pilot processing trials are often conducted with design of experiments and process optimization to make production samples for quality assurance testing.

The methodology is demonstrated with data and discussion of two industrial recycled polypropylenes having similar MFRs of 5–10 g/10 min at 230°C. The described results will show that these basic steps are insufficient to characterize the processing and quality behavior of recycled polyolefins. As such, the center column proposes further characterization including capillary rheology, differential scanning calorimetry (DSC), Fourier-transform infrared spectroscopy (FTIR), and modeling/simulation. More advanced techniques including oscillatory rheometry, microscopy, mechanical testing, and other techniques are also optionally used to investigate unexpected behaviors. Furthermore, we acknowledge and are pursuing other methods such as SAXS/WAXS,[18–20] chromatography,[21–23] and nuclear magnetic resonance (NMR,[24–26]) for comparative purposes but focus on more commonly applied methods in this article.

2 | EXPERIMENTAL

2.1 | Material safety data sheets

Two recycled polypropylene grades, referred to as PP1 and PP2, are the subject of this investigation. The material safety data sheet (SDS) for PP1 identifies the material as EEI H700-12 polypropylene resin produced by EEI Recycling (St. Petersburg, FL) while the SDS for PP2 identifies the material as ITRA-PP-REPRO-Car Grade produced by Intramex (Monterrey, Nuevo Leon, Mexico). Both materials were provided in bulk quantities (hundred-pound drums) from Geon Performance Solutions (Avon Lake, OH). For characterization and validation purposes, virgin grades of PP homopolymer (Muehlstein Certene PHT-4, Wilton, CT referred to as vPP), HDPE (Borealis BorPure MB7541, Vienna, Austria referred to as

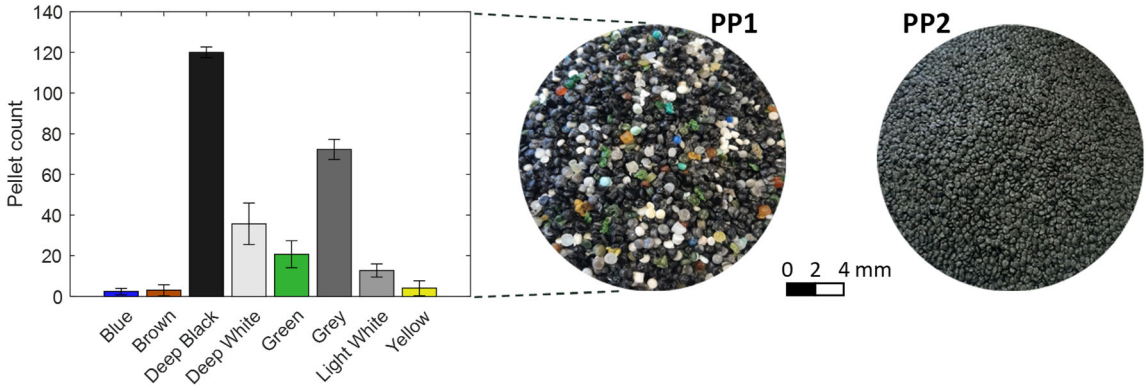

FIGURE 1 Images of polyolefin recyclates (left) PP1 and (right) PP2.

vHDPE), and an equal mass-fraction blend of these two virgin materials (referred to as vPP + vHDPE) were also processed by cast film extrusion and characterized by DSC and FTIR.

2.2 | Visual inspection

Figure 1 provides representative images of the received recyclates. PP1 is composed of granulates of varying sizes and colors while PP2 is uniformly compounded and extruded as finer granules. Accordingly, PP2 is at first objectively perceived as a higher quality material. To characterize the types of materials constituting PP1, the bar chart at left provides the pellet counts within three randomly collected PP1 samples weighing 10 g. The predominant material is a black polyolefin followed by a gray, deep (bright) white, and several other colors. DSC is later performed for these most predominant pellet types as well as the PP1 and PP2 films.

3 | RESULTS AND DISCUSSION

3.1 | Melt flow rate characterization

The two materials' melt flow rates (MFR) were characterized per ASTM D1238 with a 2.16 kg weight at 230°C resulting in respective MFRs of 8.63 ± 0.05 and 5.67 ± 0.12 g/10 min for PP1 and PP2. Both materials were within the range of 5–10 g/10 min as requested of the material suppliers for application to film extrusion (the focus of the acknowledged research support). Table 2 provides a summary of these melt flow rates and other characterized rheological models as later discussed. Given that the MFR values fell within the expected range, extrusion trials proceeded.

3.2 | Cast film processing trials

Cast film processing trials were conducted on a multi-layer extrusion system with five extruders feeding a feedblock enabling 9-layer films (Dr. Collin Teachline, Maitenbeth, Germany). Each extruder has a screw diameter of 30 mm and a length of 810 mm (a 27:1 length:diameter ratio). To characterize the processing behavior of the recyclates, only the extruder providing the central core layer was operated with each material. All forward barrel zones, feedblock, and die temperatures were set to 230°C. The extruder screw speed was set to 30 RPM, and the process allowed to equilibrate for 1 h before collecting processing data and film samples for 1 h. The extruded film was cast onto a three-roll stack having a take-off speed of 1.6 m/minute.

The melt pressure observations and pictures of extrudate film samples are provided in Figure 2. The estimated mean ± standard deviation of the die pressures was 16.74 ± 1.72 bar for PP1 and 23.91 ± 0.71 bar for PP2. A two-sample *t*-test with unpooled variance estimates was performed on these observed die pressures indicating that the plotted extrusion pressures were statistically different ($p \sim 0$, $t = 222.3$) with a likely mean difference of 7.17 bar. The ratio of the die pressures for PP2 to PP1 is 23.91/16.74 and equals 1.43. This ratio is generally consistent with expectations based on the MFR of PP1 to PP2, which is 8.63/5.67 and equals 1.52. The processing data including the plotted pressures and several other acquired processing states are available as described in the data availability statement.

The extruded film for PP1 was stable with uniform color and thickness on the order of 0.06 mm. By comparison, the outlet melt velocity across the die varied so much for PP2 that the film immediately separated prior to entering the roll stack resulting in the two narrower and

TABLE 2 Comparison of two recycled polypropylenes.

Material	**PP1**		**PP2**	
MFR (g/10 minutes, 2.16 kg)	8.63 ± 0.05		5.67 ± 0.12	
Model coefficient by material and rheometry	**Capillary**	**Oscillatory**	**Capillary**	**Oscillatory**
Oscillatory crossover modulus [kPa]	N/A	30.1	N/A	39.6
Oscillatory crossover frequency [rad/s]	N/A	266.1	N/A	153.5
Willamson, zero shear viscosity, η_0 (230°C) [Pa]	1127	868	1935	2662
Willamson, power-law index, n	0.249	0.317	0.283	0.352
Willamson, consistency index, k [s]	0.0232	0.0623	0.0437	0.2141
Willamson, 1-n	0.751	0.683	0.717	0.648
Cross-WLF, n	0.280	0.280	0.274	0.274
Cross-WLF, τ[a]	37,700	37,700	50,600	50,600
Cross-WLF, D1	4.76E+20	4.76E+20	7.58E+20	7.58E+20
Cross-WLF, D2	153	153	153	153
Cross-WLF, A1	46.4	46.4	46.7	46.7
Cross-WLF, A2	51.6	51.6	51.6	51.6
Cross-WLF, η_0 (230°C) [Pa]	1303	1303	1597	1597
Williamson, D1 adjusted	4.118E+20	3.172E+20	9.183E+20	1.263E+21
COMSOL, equation for Eta0[a]	4.118E+20*exp(−46.4*(ht.T-153)/(51.6 + ht.T-153))			
Williamson, η_0 (230°C) verification [Pa]	1127	868	1935	2661.3

[a]Equation is provided as an example of the temperature dependence of the zero shear viscosity for the Williamson-WLF model using the PP1 coefficients fitted to the capillary data.

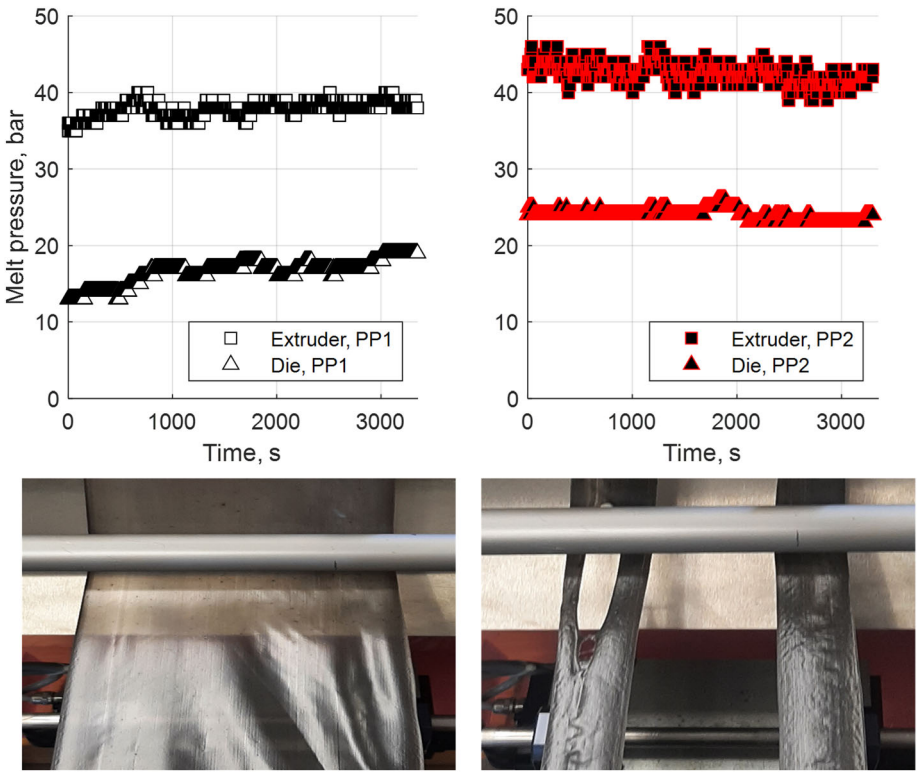

FIGURE 2 (top) Melt pressure at the extruder outlet and die inlet as well as (bottom) images of extruded films for (left) PP1 and (right) PP2.

thicker strips shown at bottom right in Figure 2. Each of the two PP2 strips exhibited a rougher surface and greater thickness variation than the PP1 film. The results seemed surprising given that PP1 was the feedstock with varying size and color of pellets (see Figure 1). Accordingly, further material characterization was performed to explain and mitigate the variation in the extruded film exit velocities.

3.3 | Capillary and parallel plate rheology

Capillary rheology was performed to characterize the shear viscosity as a function of the apparent shear rate in the materials. While many corrections can be performed to account for end effects, non-Newtonian behavior, pressure, and other effects,[27–29] the focus here is to perform capillary rheometry as typically applied in industry practice. Accordingly, the rheological properties of the PP1 and PP2 materials were characterized by a capillary rheometer (Dynisco LCR 7600, Franklin, MA) having a capillary die with a bore diameter of 1 mm and bore length of 30 mm. Given the processing temperature of 230°C, the capillary rheometry was performed for melt temperatures of 210, 230, and 250°C. The materials were tested as received without prior compounding of the disparate recyclates comprising PP1. Prior to plunger displacement, the materials were brought to the target melt temperatures and allowed to equilibrate for 7 min (420 s) after which a geometrically decreasing shear rate profile was implemented according to ASTM D3835. Transient fluctuations in the melt pressure due to inconsistencies in the melting and flow of the granulated feedstock of PP1 were not observed. This capillary viscosity data are openly available as described in the data availability statement.

The characterized shear viscosity as a function of the apparent shear rate at the wall is plotted in Figure 3 for PP1 (unfilled triangles) and PP2 (black-filled triangles). The PP1 and PP2 melts have generally similar shear viscosity behaviors with PP2 exhibiting a higher viscosity than PP1 as consistent with their MFR values. To quantify these behaviors, a Williamson model[30] is fit to the data using a Matlab script available with the viscosity data. While there are many excellent shear viscosity models,[30–35] the Williamson model was chosen in this research since it is the simplest viscosity model that explains the observed behavior to high fidelity while also providing intuitive model coefficients. The Williamson model has the form:

$$\eta(\dot{\gamma}) = \frac{\eta_0}{1 + (k\dot{\gamma})^{1-n}}. \quad (1)$$

here, η_0 represents the Newtonian (zero shear rate) viscosity at the processing temperature of interest (230°C),

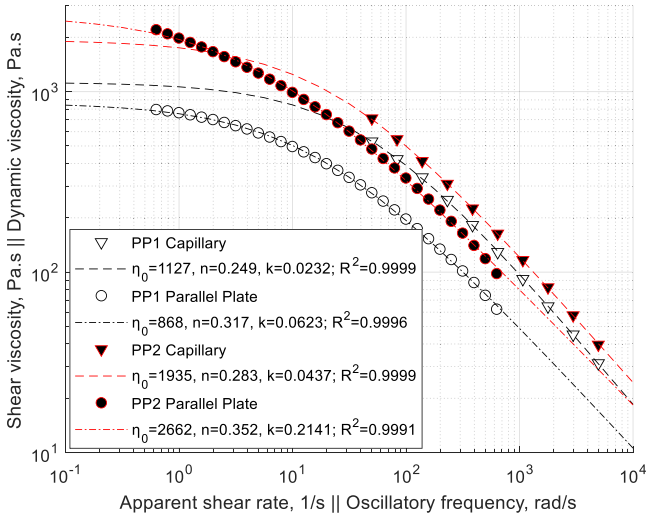

FIGURE 3 Rheology data and model fits for PP1 (white-filled and black-outlined) and PP2 (black-filled and red-outlined) as tested by capillary rheometry (triangular symbols) and parallel plate rheometry (circular symbols).

n is the power-law index, and k is a characteristic relaxation time. Table 2 and the legend of Figure 3 provide the corresponding model coefficients and statistics. The ratio of the zero shear rate viscosities for PP2/PP1 are 1935/1127, which equals 1.72 and is generally consistent with the ratio of the MFRs for PP2/PP1 equaling 1.52. The moderate discrepancy between the two ratios is due to the shear-thinning behavior of the materials though, critically, the capillary data suggest that the characteristic relaxation time of 0.0437 s for PP2 is approximately twice the 0.0232 s for PP1. While there are some differences in the capillary viscosity behaviors and model coefficients, capillary rheology does not explain the observed extrusion behavior of Figure 2.

A literature review of melt instabilities[36,37] suggested that an increased storage modulus, G′, can act as a primary driver through the accumulation of elastic stresses in melt processing. Accordingly, parallel plate rheology was also performed. An Auto Series 4394 ASTM Automatic Hydraulic Laboratory Press (Carver, Wabash, IN) with platen temperature and clamp force profiling was used to produce rheological samples of approximately 2 mm in thickness and 25 mm in diameter from stacked PP1 and PP2 films. The samples' dynamic rheological behavior was analyzed using a TA Instruments ARES-G2 rheometer (New Castle, DE). Each sample was temperature equilibrated for 90 s, followed by a 10% stepwise reduction in the gap before the testing position was attained (approximately 1.4 mm) to ensure proper filling of the parallel plate geometry and accurate trimming of the sample edge. A strain sweep was then performed at 230°C between strain amplitudes of 0.2% and 50% to determine the linear

viscoelastic limit before the frequency and time-dependent studies. A strain amplitude between 1% and 10% within the linear viscoelastic limit was selected for dynamic frequency and time sweep measurements. A time sweep was also conducted with the PP1 and PP2 materials to verify stability of the melt behavior for 1800 s at 230°C.

The rheological behavior of PP1 and PP2 as characterized by the parallel plate rheometer are, respectively, shown by the open circles and black-filled circles in Figure 3. The fitted Willamson model coefficients are also provided in that figure's legend as well as Table 2; the supplemental information provides the full data set including the storage and loss modulus, G′ and G″. The PP1 and PP2 behaviors are characterized by capillary and parallel plate rheometers are generally consistent. However, the parallel plate rheometer tends to predict higher zero shear rate viscosities as well as higher characteristic relaxation times, k. Perhaps the single biggest difference is that the 0.2141 s value of k for PP2 is more than three times the 0.0623 s value estimated by capillary viscometry and nearly five times the 0.0437 s characterized for PP1.

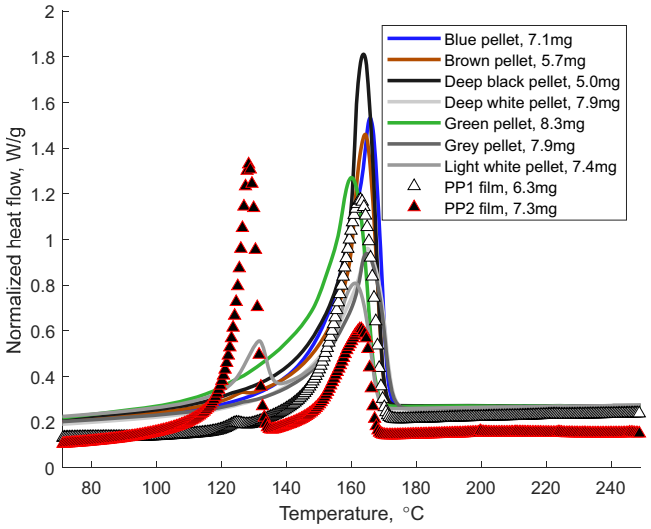

FIGURE 4 Measured heat flow data for constitutive materials of PP1 (colored per filled bars of Figure 2), PP1 film (white-filled and black-outlined triangles), and PP2 (black-filled and red-outlined triangles).

3.4 | Thermal characterization (DSC, thermogravimetric analysis)

To identify varied constituents in the recycled PP materials, both DSC and thermogravimetric analysis (TGA) were performed. The DSC was performed on the extruded PP1 and PP2 films as well as the most common pellets constituting the mix of the PP1 feedstock (see Figure 1). For each material, the DSC was performed with a heating, cooling, and second heating cycle with a temperature ramp rate of 10°C/minute per ASTM D3418 using a differential scanning calorimeter 3+ (Mettler Toledo, Columbus, OH). Figure 4 provides the normalized heat flows for the second heat cycle (endothermic up) of the characterized samples wherein (1) the measured heat flow is divided by the sample mass indicated in the legend, and (2) the heat flows for the varying colored pellets constituting the PP1 film are normalized to the PP1 film at the melt temperature of 230°C. The results are interesting in that they demonstrate different peaks in their melting behavior around 165°C indicative of different PP molecular weight (MW) distributions as well as secondary peaks around 125°C indicative of PE contamination.

Analysis of the heat flows can be used to estimate the PP and PE content of the PP1 and PP2 films.[38] The approach is to evaluate the relative of melting enthalpies of the PE and PP constituents using calibration curves for DSC[39] or temperature modulated DSC[13] with subsequent analysis.[40] Here, a Matlab script (available in the open data DSC folder) was developed to estimate the amorphous PE behavior for each material as plotted in Figure 5. The calculation of the amorphous behavior was performed by linear interpolation between the two corners of the PE melting peak; the interpolated behavior closely follows that of amorphous PE as characterized by Gaur and Wunderlich.[41] The melting enthalpy, ΔH, was then calculated as the area between the normalized heat flow curve and the amorphous behavior for PP1 and PP2 using trapezoidal numerical integration; these melting enthalpies were, respectively, calculated as 0.475 J/g for PP1 and 59.1 J/g for PP2.

The local melting peaks of the PE constituents were identified indicating that the peak of 128.3°C for PP2 corresponds to HDPE with a density around 950 kg/m^3 while the lower peak of 124.7°C for PP1 corresponds to predominantly LLDPE contamination with a density around 930 kg/m^3.[13] Based on a set of 8 calibration curves varying PE content from 100 to 0% in PP/PE blends,[39] the fraction of PE in PP1 and PP2 is estimated as $PE = 0.753\Delta H + 2.69$ resulting in estimates of 3.1% LLDPE in PP1 and 47.1% HDPE in PP2. For validation purposes, the same calibration model was applied to the three film grades of vPP, vPP + vHDPE, and vHDPE with respective estimates of 2.69%, 49.7%, and 104.1% PE. It is also observed that the PP1 recyclate generally matches the vPP while the PP2 recyclate generally matches the vPP + vHDPE blend. These results suggest that DSC provides a reliable if approximate method to estimate the PE fraction in PO blends based on melting enthalpy.

TGA was also implemented with a Mettler Toledo TGA 2 DF (Columbus, OH) at temperature ramp rates of 10 and 100°C/minute. The top subplot of Figure 6 provides the mass loss while the bottom subplot provides the rate of mass loss for the PP1 and PP2 specimens at a temperature ramp of 100°C/minute. Two TGA tests were conducted for each of the PP1 and PP2 films; the individual traces were found to be similar, and so, the average of the two tests is reported in Figure 6 for PP1 and PP2. The PP1 and PP2 mass loss trajectories have very similar behaviors, but analysis of the data suggests that PP1 has a peak degradation temperature of 483.3°C with residual mass of 1.09% while PP2 has a peak degradation temperature of 485.0°C with residual mass of 1.97%. Interestingly, the temperature ramp rate of 10°C/minute yielded greater variances in the peak temperatures with PP1 having a peak degradation temperature of 458.8°C and residual mass of 0.26% while PP2 had a peak degradation temperature of 465.7°C with residual mass of 1.19%. While this latter data set is not plotted in Figure 6, all data and analysis codes are available in the open data.

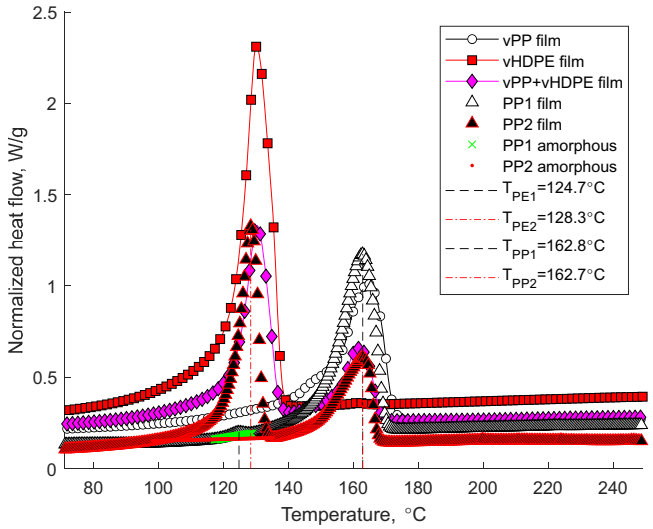

FIGURE 5 Heat flow data for vPP, vHDPE, vPP + vHDPE blend, PP1, and PP2 with indicated peaks and amorphous behavior.

The temperature ramp rate of 100°C/minute was chosen to match the pyrolysis conditions of Xi et al who[42] investigated the degradation of various plastics including LDPE and PP. Xi found that LDPE in their setup has a peak degradation temperature of 508°C with residual mass of 1.09% while PP has a peak degradation temperature of 491°C with residual mass of 0.85%. Xi's results suggest that the peak degradation temperature should increase 0.17°C per percent weight increase in PE content. Both the peak degradation temperature and residual mass of PP1 and PP2 indicated in Figure 6 are qualitatively consistent with Xi's results. However, the change in the peak degradation temperature between PP1 and PP2 is only 1.7°C which would be indicative of only a 10% increase in PE content for PP2. It may seem that using pyrolysis data for LDPE would be a poor substitute for HDPE, but the research literature shows that the two materials have identical peak degradation temperatures.[43,44] Instead, the primary reason for the

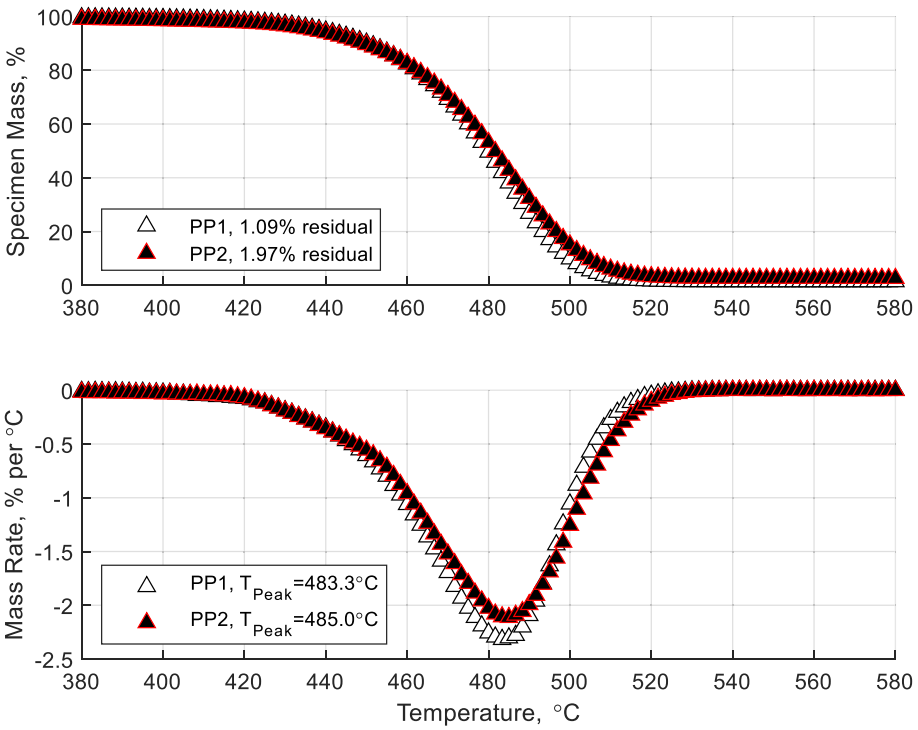

FIGURE 6 (top) Mass loss and (bottom) rate of mass loss for PP1 and PP2 specimens at a temperature ramp of 100°C/minute.

discrepancy in our results with those of Xi is likely that the pyrolysis rate is not linear with the blend ratio. Given the increased sensitivity of our results at the lower temperature ramps rate of 10°C/minute, it may be that calibration curves and test protocols can be developed to identify the PE content in PP/PE blends.

3.5 | Fourier-Transform Infrared Spectroscopy

To evaluate potential online characterization methods, FTIR was performed with a Thermo Fisher Scientific Nicolet iS50 (Waltham, MA) in both reflective and attenuated total reflectance (ATR) modes. The spectrum was characterized for each of the cast PP1 and PP2 films as well as the cast vPP, vHDPE, and vPP + vHDPE blend films between wavenumbers of 400 and 4000 cm^{-1} in increments of 0.48 cm^{-1}. Following the recommendation of Islam et al,[45] each of the spectra was lightly filtered using the Matlab function filtfilt() with a first-order, low-pass Butterworth filter having a cutoff frequency of 0.2; this filter is similar to use the averaging of five adjacent observations such as implemented by the Matlab function smooth(). The absorbance spectra were then baselined by subtracting the average of the characterized absorbance at wavenumbers near 1200 and 1600 cm^{-1} per ASTM D7399.[46]

Three different FTIR estimation models were used to evaluate the PP fraction in PP1 and PP2. First, ASTM D7399[46] was used to evaluate the ratio, r, of the peak absorbance near wavenumber 1378 cm^{-1} (characteristic of methyl (CH_3) bending vibrations common in PP) to the peak absorbance near wavenumber 1465 cm^{-1} (characteristic of bending mode of the CH_2 group present in both PE and PP); this ASTM method is practically equivalent to that described by Agilent using the peak ratio of 1376/1462 cm^{-1}.[47] Our absorbance spectra characterized in transmission mode are shown in the top left subplot of Figure 7 with these characteristic peaks. Per ASTM D7399, a linear calibration model relating this absorbance ratio to the mass fraction of PP, x, was fitted to the absorbance spectra of the cast vPP, vHDPE, and vPP + vHDPE blend resulting in $r = 0.00399 + 0.0178x$ with an adjusted coefficient of determination, R^2, of 0.9935. This fitted model estimates a fraction of 56.1% PP in PP1 and 42.2% of PP in PP2 as shown in the top right subplot of Figure 7.

A second FTIR estimation model is based on Camacho and Karlsson[48] who suggest an absorbance ratio, $r = A(1168)/[A(1168) + A(720)]$, based on the rationale that the absorbance near a wavenumber of 1168 cm^{-1} is characteristic of "methyl group wagging in PP" while the peak near 720 cm^{-1} arises from "methylene rocking typical for HDPE." Camacho and Karlsson's model resulted in an R^2 of 0.9987 with $r = 4e\text{-}5x^2 + 0.0058x$ wherein x is the mass fraction of PP in a PP-PE blend. Our absorbance spectra as characterized in transmission mode are shown in the middle left subplot of Figure 7 with these characteristic peaks. Per Camacho and Karlsson, a pure quadratic calibration model relating this absorbance ratio to the mass fraction of PP was fitted to the absorbance spectra of the cast vPP, vHDPE, and vPP + vHDPE blend resulting in an $R^2 \sim 1$ with $r = 1.18e\text{-}4x^2\text{-}1.25e\text{-}3x$ (leaving one degree of freedom for estimation of R^2). This second fitted model estimates a fraction of 96.5% PP in PP1 and 51.5% of PP in PP2 as shown in the middle right subplot of Figure 7.

The third FTIR estimation model is based on Xiao and Ernst[49] using ATR mode with an attenuation ratio of the PE peak centered at 719 cm^{-1} (attributed to methylene group rocking) to the PP peak centered at 1376 cm^{-1} (attributed to methyl group symmetrical bending) for a linear estimate of the PP fraction. Our absorbance spectra as characterized in ATR mode are shown in the bottom left subplot of Figure 7 with these characteristic peaks. Per Xiao and Ernst, a linear calibration model relating this absorbance ratio to the mass fraction of PP was fitted to the absorbance spectra of the cast vPP, vHDPE, and vPP + vHDPE blend resulting in $r = 3.84\text{–}0.0407x$ with an $R^2 \sim 0.9$. This third fitted model estimates a fraction of 79.5% PP for both PP1 and PP2 as shown in the bottom right subplot of Figure 7.

In addition to the estimation models plotted at right in Figure 7 based on our FTIR characterization data, the PP fractions were also estimated using model coefficients in the literature. Use of the model coefficients from Camacho and Karlsson[48] with our FTIR data results in an estimated PP fraction of 91.2% in PP1 and 51.9% in PP2. Larsen et al[39] also provide an estimation model having the form $x = 1.209r^2\text{-}0.218r$ that results in an estimate of 98.0% PP in PP1 and 69.3% PP in PP2. These results suggest that FTIR based on the absorbance ratio, $r = A(1168)/[A(1168) + A(720)]$, provides robust estimates of the PP composition in the PP1 and PP2 recyclates.

3.6 | Observability of PP/PE blends

Table 3 summarizes the estimated PP mass fractions in the PP1 and PP2 grades. DSC ostensibly offers the highest fidelity approach using the second heat cycle given estimated melting enthalpies-specific grades of PE (LLDE, LDPE, and HDPE) identified from the peak melting temperature. However, the DSC is an off-line characterization technique and so not readily amenable to continuous process monitoring needed for real-time control. By comparison, FTIR offers an online

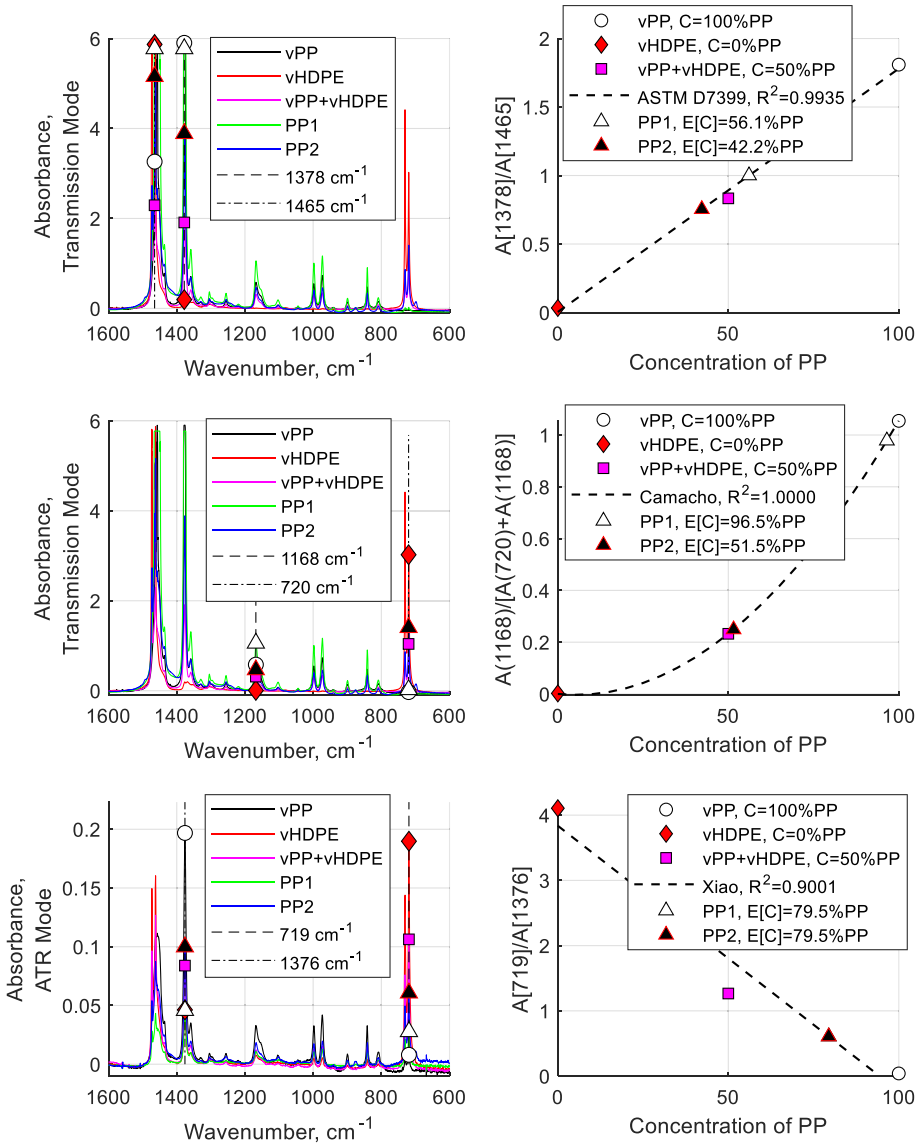

FIGURE 7 (left) FTIR spectra of vPP, vHDPE, vPP + vHDPE, PP1, and PP2 with evaluated peaks, and (right) fitted models per (top) ASTM D7399,[46] (middle) Camacho and Karlsson,[48] and (bottom) Xiao and Ernst.[49]

TABLE 3 Comparison of PP weight fractions for PP1 and PP2.

Method	PP1	PP2
DSC, UML based on [24]	97.0	53.8
DSC, JHU based on [10]	99.6	59.6
DSC, JHU, based on [24]	96.9	40.7
TGA, Xi et al[42]	~100	~90
FTIR, ASTM D7399 w/UML Calibration	48.8	38.2
FTIR, Camacho and Karlsson[48] w/UML Calibration	98.0	52.5
FTIR, Xiao and Ernst[49] w/UML Calibration	78.5	78.5
FTIR, Camacho and Karlsson[48]	91.2	51.9
FTIR, Larsen et al[39]	98.0	69.3

alternative approach for continuous characterization of the extruded films though there are some significant variations in the PP/PE blend estimates for the PP1 and PP2 materials resulting from the application of different characteristic peaks and analysis methods.

A critical issue is that the exact PP/PE blend morphology varies as a function of time and space during the polymer processing operation such that there is always some variation within the PP1 and PP2 melts and, thus, also within the extruded film samples as a function of its length, width, and thickness locations. The implication is that the properties of the film may vary in a significant manner that would be unknown without continuous monitoring and, thus, uncontrolled. Twin screw extrusion offers both dispersive and distributive mixing to mitigate local PE/PP variations while also allowing the tuning of

the PE/PP blend percentage through compounding with known grades.[50,51] However, this additional compounding step adds cost in the form of labor, energy, and carbon footprint while not guaranteeing the blend properties (e.g., the poor film extrusion of PP2 that appears homogeneous). Accordingly, there is further need for modeling to understand and control the melt instability observed in Figure 2.

3.7 | Modeling

A series of non-Newtonian flow simulations, both isothermal and non-isothermal, were conducted using COMSOL 6.1 (Stockholm, Sweden) to understand the melt flow behavior. The modeled geometry for the film die is shown in Figure 8 as created in SolidWorks (Waltham, MA) from die drawings provided with the Dr. Collin multi-layer film extrusion line. The geometry of the internal flow channels are based on the Winter-Fritz die,[52] also widely referred to as a coat hanger or horseshoe design. The design intent is to provide a rearward distributor section near the die inlet before a forward flat (slit) section of constant thickness so that the extrudate flows uniformly across the width of the die with minimal variances related to changes in flow rate and melt viscosity. The modeled die has an inlet that is 40 mm wide and 9.4 mm thick while the slit geometry at the die outlet is 250 mm wide with a thickness of 1.4 mm.

A quarter model mesh was created using symmetry conditions defined on the vertical and horizontal center planes of the die. Physics-based (for fluid flow) meshing was prescribed with defined eight boundary layers on the external surfaces and two additional boundary layers on the horizontal symmetry plane to ensure at least 10 layers through the half thickness. The resulting mesh comprised 522,274 mixed elements (tetrahedra, pyramids, prisms, and hexahedra); portions of the mesh are illustrated in Figure 8 near the die inlet at right and outlet at left. A custom viscosity model was defined based on the Williamson model of equation (1) with the coefficients of Table 2 for the various rheological characterizations. The WLF temperature dependence was implemented for non-isothermal simulation by modeling the Williamson zero shear rate viscosity coefficient based on WLF model coefficients fitted by capillary viscometry at 210, 230, and 250°C. Table 2 also provides the cross-WLF model and non-isothermal coefficients as well as an example COMSOL equation defining the zero shear rate viscosity based on the PP1 capillary data.

Six different simulations of varying conditions and increasing complexity were modeled as detailed in Table 4. While the same mesh was used for all simulations, the number of degrees of freedom and compute time vary with the assumptions and processing conditions. Figure 9 provides the six sets of simulation results with varying material constitutive models, assumptions, and process settings. The top view at left in each set includes the velocity vectors on the horizontal center plane of the die as well as the temperature contours on the horizontal center plane for non-isothermal simulations; the contour plot at right in each set depicts the melt exit velocity normal to the die lip. Sets (a) and (b) compare the PP1 and PP2 melt flows based on capillary data assuming isothermal conditions with a uniform inlet velocity U equal to 4 mm/s. It is observed that the capillary viscosity characterization results in very similar flow fields for PP1 and PP2, though inspection of the velocity contours at right of each set predicts that PP2 has a slightly more non-uniform velocity field. Sets (b) and (c) compare the velocity field prediction for PP2 with capillary and

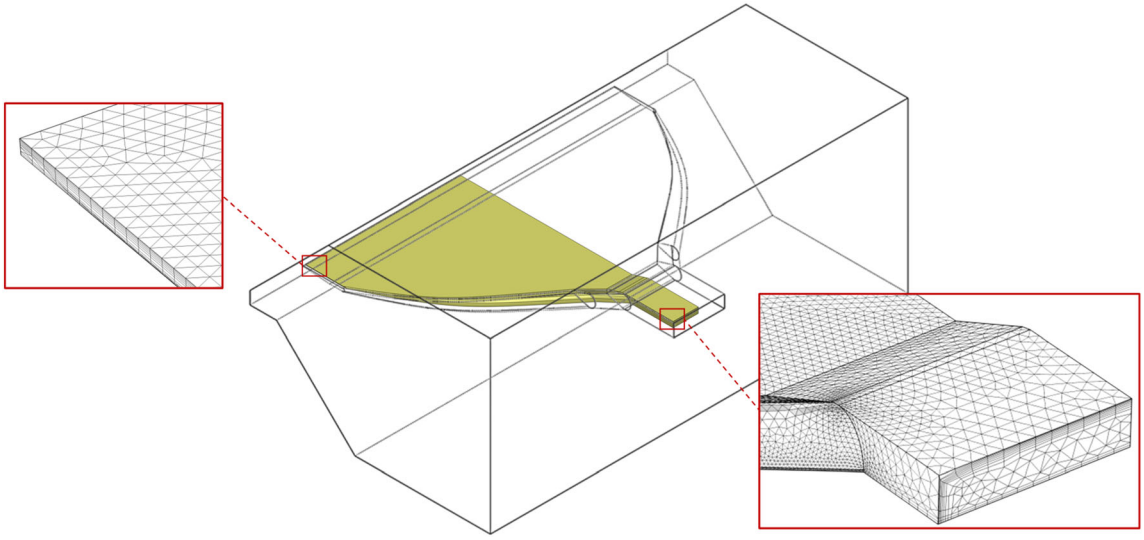

FIGURE 8 Geometry of coat hanger film die showing quarter-symmetry model and mesh details.

TABLE 4 Simulation conditions and compute requirements.

Simulation condition	(a)	(b)	(c)	(d)	(e)	(f)
Material	PP1	PP2	PP2	PP2	PP2	PP2
Viscometry	Capillary	Capillary	Oscillatory	Oscillatory	Oscillatory	Oscillatory
Isothermal?	Yes	Yes	Yes	No	No	No
Inlet and die temperature,°C	230	230	230	230	230	230
Heat transfer coefficient, W/m^{2}K	N/A	N/A	N/A	500	50	50
Die inlet velocity, mm/s	4	4	4	4	4	20
Mesh elements	522,274	522,274	522,274	522,274	522,274	522,274
Degrees of freedom	845,724	845,724	845,724	1,057,155	1,057,155	1,057,155
Memory, GB	9.56	9.56	9.60	12.73	12.68	12.82
Compute time, s	353	416	416	5102	6402	8468

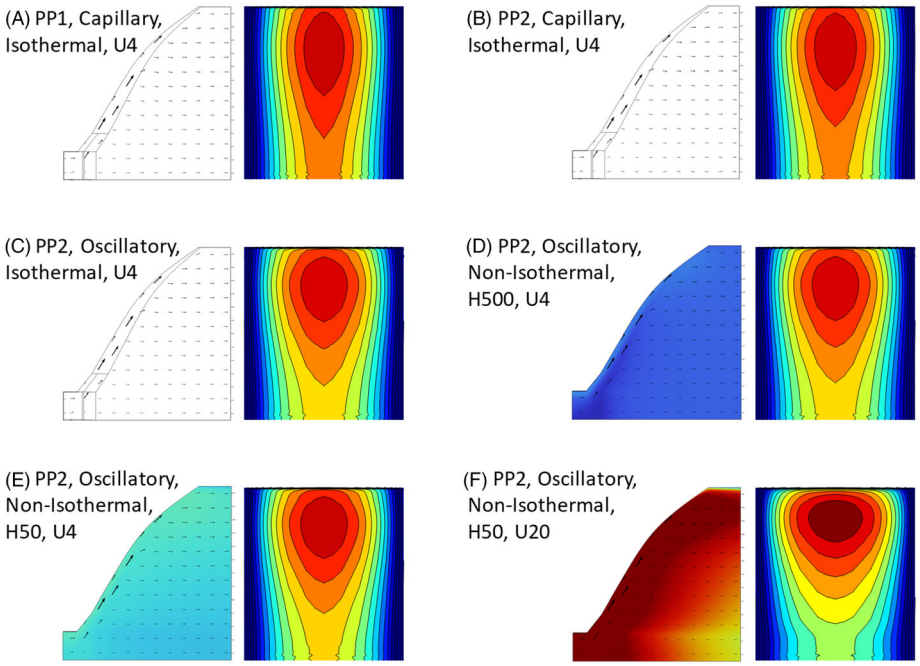

FIGURE 9 Sets of simulation results (A) to (F) per conditions of Table 3 including velocity vectors and temperature distribution at left and normal exit velocity contours at right.

parallel plate rheological data. This set of results shows that the parallel plate data models greater flow variation across the die lip from the edge of the die to the center. Reviewing the rheology data of Figure 3 and viscosity model coefficients of Table 2, the likely reason for the greater disparity is the higher Newtonian viscosity. More specifically, the flow resistance in the thinner slit section between the distributor section and the die lip will have zero shear rates on the horizontal center plane. With a higher Newtonian viscosity being modeled, the parallel plate data will tend to drive a greater proportion of the flow away from the slit section that has the longest flow path with relatively higher apparent flow resistance.

Sets (C) and (D) of Figure 9 compare the effect of the non-isothermal assumption with set (D) modeling a heat transfer coefficient (HTC) of 500 W/m^{2}K between the melt and the external die surfaces. This value of the HTC was chosen from a recent literature review and meta-analysis of thermal contact resistance[53] so as to be representative of heat transfer conditions at moderate pressures observed in the observed extrusion process (e.g., 20 MPa at the die inlet shown in Figure 2). Somewhat surprisingly, the relaxation of the isothermal assumption did not significantly affect the flow distribution. The likely reason is that the temperature variation from the coldest to hottest region was on the order of 1°C, indicating that the heat conduction to the die was able to largely dissipate the viscous heating of the flowing melt. When the HTC is reduced from 500 W/m^{2}K in set (D) to 50 W/m^{2}K in set (E), the temperature variation increases the melt temperature in the rearward distributor section by 5°C. This increased temperature reduces the

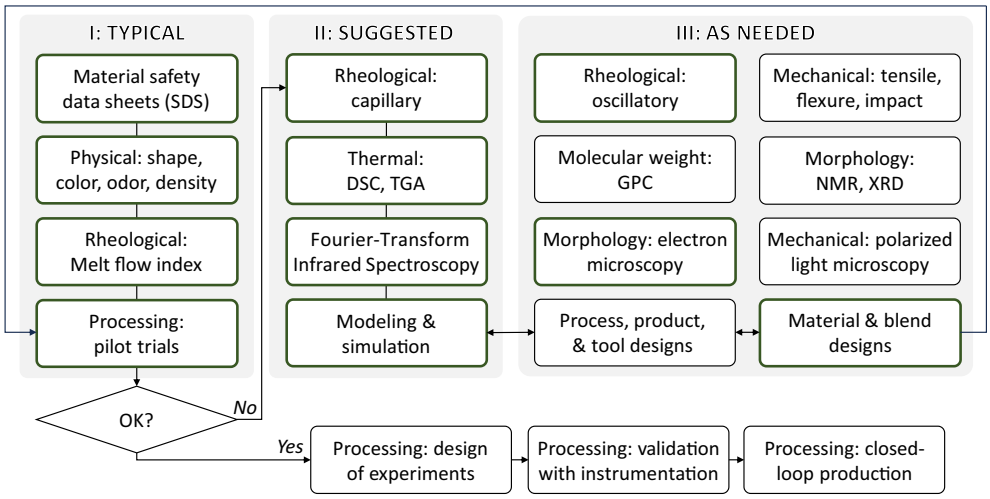

FIGURE 10 Overview of material characterization and modeling protocol.

melt viscosity in the distributor section and, thus, drives slightly greater variation in the exit melt velocities.

Set (F) of Figure 9 investigates the effect of increasing the inlet melt velocity, U, to 20 mm/s, a five-fold increase from that of set (E). The resulting velocity field at the die exit is markedly different with an extra dark red contour showing much higher velocity near the sides of the die and two extra lower contours (yellow and green) showing lower velocities near the center of the die. The increased variance in the melt exit velocities is predominantly driven by the shear-thinning behavior of the viscosity. Specifically, higher shear rates will occur throughout the die, but the higher velocities in the thicker flow distributor causes increased melt temperatures, lower viscosities, and thus greater variation in the exit flow velocities. By comparison, Newtonian viscosities on the horizontal center plane of the thinner slit section will tend to maintain the flow resistance relative to the lower flow resistance in the distributor section associated with the lower melt viscosities driven by additional shear thinning and viscous heating.

4 | CONCLUSIONS

There are two sets of broad conclusions that are drawn. First, the characterization work suggests that melt flow rate is a poor predictor of material consistency. DSC provides the highest fidelity characterization approach for modeling the material constituents with the ability to predict not only the relative fraction of PE in a PP recyclate, but also the type of PE (HDPE, LDPE, LLDPE) from the peak melting temperature. However, DSC is traditionally a laboratory technique. FTIR provides a reasonably high-fidelity approach, though calibration functions need to be validated on an application-specific basis. TGA as well as capillary and oscillatory rheometry are able to capture significant differences between grades of recycled polyolefins but provide aggregate behaviors of the materials rather than detailed constituent information.

The second conclusion goes to the diagnosis and remedy of variations in recycled polyolefins. While the modeling elucidates the effects of the viscosity characterization method, non-isothermal assumption, and process settings, the simulations failed to reproduce the extent of the variation that were observed in processing of two industrial polyolefins with relatively similar melt flow rates and viscosity behaviors. The concern is that, from a practical point of view, there is no obvious predictor of the processing issues that may occur prior to actual processing of the recycled polyolefins. Thus, processors must rely on instrumentation suites that reliably diagnose the defect modes as well as human expertise to remedy the variations in recycled polyolefins. Accordingly, current research efforts are directed to implementation of a camera-based film thickness estimator and continuous FTIR detector to provide feedback for automatic adjustment of solids blending and process settings towards the detailed design and validation of the bottom row of control functions indicated in Figure 10.

ACKNOWLEDGMENTS

This work is supported by the National Science Foundation (NSF) under Grant #2118808, DMREF/Collaborative Research: Integrated Material Design and Processing—Application to Recycled Plastics, 12/1/2021 to 11/30/2025. Any opinions, findings, and conclusions or recommendations expressed in this material are those of the author(s) and do not necessarily reflect the views of the NSF. Additionally, the authors acknowledge the National Institute of Standards of Technology for guidance on some of the employed techniques. The authors would also like to thank Geon Performance Solutions (Avon Lake, OH) for the provision of the recycled materials.

CONFLICT OF INTEREST STATEMENT

The authors declare no competing interests. One of the authors, D. Kazmer, of this article is part of the Editorial Board of the journal. To avoid potential conflicts of interest, that author had no access to confidential information related to the editorial process of this article.

DATA AVAILABILITY STATEMENT

The data that support the findings of this study are openly available in the Platform for the Accelerated Realization, Analysis, and Discovery of Interface Materials (PARADIM) at https://data.paradim.org/doi/k1mm-cf38/.

ORCID

David O. Kazmer https://orcid.org/0000-0002-1166-4043
Sixtus O. Nzeh https://orcid.org/0009-0002-6639-2476
Margaret Sobkowicz-Kline https://orcid.org/0000-0003-0571-0952

REFERENCES

1. OECD. *Global Plastics Outlook: Economic Drivers, Environmental Impacts and Policy Options*. OECDiLibrary; 2022:201. doi: 10.1787/de747aef-en Accessed March, 2024.
2. *Global Plastics Outlook: Economic Drivers, Environmental Impacts and Policy Options*. Organisation for Economic Cooperation and Development (OECD); 2022.
3. Lebreton L, Andrady A. Future scenarios of global plastic waste generation and disposal. *Palgrave Communications*. 2019;5(1):1-11.
4. Geyer R, Jambeck JR, Law KL. Production, use, and fate of all plastics ever made. *Sci Adv*. 2017;3(7):e1700782.
5. Polyportis A, Magnier L, Mugge R. Guidelines to Foster consumer acceptance of products made from recycled plastics. *Circular Economy and Sustainability*. 2023;3(2):939-952.
6. Shi J, Jiang Z. Willingness to pay a premium price for green products: does a reference group matter? *Environ Dev Sustain*. 2023;25(8):8699-8727.
7. Lander E et al. *Materials Genome Initiative Strategic Plan*. National Science and Technology Council; 2021 https://www.mgi.gov/sites/default/files/documents/MGI-2021-Strategic-Plan.pdf Accessed February, 2024
8. Lander E, Koizumi K. *Materials Genome Initiative Strategic Plan*. U.S. National Science and technology Council; 2021.
9. Wilkinson MD, Dumontier M, Aalbersberg IJJ, et al. The FAIR guiding principles for scientific data management and stewardship. *Scientific Data*. 2016;3(1):1-9.
10. Brinson LC, Bartolo LM, Blaiszik B, et al. Community action on FAIR data will fuel a revolution in materials research. *MRS Bull*. 2024;49(1):12-16.
11. Creations A. MatWeb: online materials information resource. Internet. http://www.matweb.com/search Accessed February, 2024
12. MatWeb: Online Materials Information Resource.
13. Scoppio A, Cavallo D, Müller AJ, Tranchida D. Temperature modulated DSC for composition analysis of recycled polyolefin blends. *Polym Test*. 2022;113:107656.
14. Richard GM et al. Optimization of the recovery of plastics for recycling by density media separation cyclones. *Resour Conserv Recycl*. 2011;55(4):472-482.
15. Bauer M, Lehner M, Schwabl D, et al. Sink–float density separation of post-consumer plastics for feedstock recycling. *Journal of Material Cycles and Waste Management*. 2018;20:1781-1791.
16. Bingham EC. *Fluidity and Plasticity*. Vol 1. McGraw-Hill; 1922:93-127.
17. Uzzi B. The sources and consequences of embeddedness for the economic performance of organizations: the network effect. *Am Sociol Rev*. 1996;61:674-698.
18. Chmelař J, Pokorný R, Schneider P, Smolná K, Bělský P, Kosek J. Free and constrained amorphous phases in polyethylene: interpretation of 1H NMR and SAXS data over a broad range of crystallinity. *Polymer*. 2015;58:189-198.
19. Schneider K, Zafeiropoulos NE, Stamm M. In situ investigation of structural changes during deformation and fracture of polymers by synchrotron SAXS and WAXS. *Adv Eng Mater*. 2009;11(6):502-506.
20. Zhong G-J, Yang SG, Lei J, Li ZM. Flow-induced polymer crystallization under pressure and its engineering application in "structuring" polymer processing. *Macromolecules*. 2024;57(3):789-809.
21. Macko T, Brüll R, Zhu Y, Wang Y. A review on the development of liquid chromatography systems for polyolefins. *J Sep Sci*. 2010;33(22):3446-3454.
22. Pasch H, Ndiripo A, Bungu PSE. Multidimensional analytical protocols for the fractionation and analysis of complex polyolefins. *J Polym Sci*. 2022;60(7):1059-1078.
23. Pasch H, Bungu PE. 20 years of polyolefin HPLC: accomplishments and challenges. *Eur Polym J*. 2023;200:112491.
24. Pasch H, Heinz LC, Macko T, Hiller W. High-temperature gradient HPLC and LC-NMR for the analysis of complex polyolefins. *Pure Appl Chem*. 2008;80(8):1747-1762.
25. Litvinov V, Men Y. Time-domain NMR in polyolefin research. *Polymer*. 2022;256:125205.
26. Kapur GS, Goel V, Luthra P, Kumar R, Tyagi H, Ramakumar SSV. Time-domain NMR relaxometery–a green analytical tool for estimating physico-mechanical properties of polyolefins. *Int J Polym Anal Charact*. 2022;27(2):111-131.
27. Negami S, Wargin R. Determination of true flow curves from capillary rheometer data. *J Appl Polym Sci*. 1968;12(1):123-129.
28. Moshe A, Kazmer DO, Johnston SP, Malloy RM, Kenig S. Analysis of variance in capillary rheometry. *Polym Eng Sci*. 2016;56(8):895-904.
29. Bagley E. End corrections in the capillary flow of polyethylene. *J Appl Phys*. 1957;28(5):624-627.
30. Williamson RV. The flow of pseudoplastic materials. *Ind Eng Chem*. 1929;21(11):1108-1111.
31. Malkin AY, Isayev A. Concepts, methods and applications. *Appl Rheol*. 2006;16(5):240-241.
32. Cross MM. Polymer rheology: influence of molecular weight and polydispersity. *J Appl Polym Sci*. 1969;13(4):765-774.
33. Williams ML, Landel RF, Ferry JD. The temperature dependence of relaxation mechanisms in amorphous polymers and other glass-forming liquids. *J Am Chem Soc*. 1955;77(14):3701-3707.
34. Ostwald W. de Waele-Ostwald equation. *Kolloid Zeitschrift*. 1929;47(2):176-187.

35. Malkin AY, Isayev AI. *Rheology: Concepts, Methods, and Applications*. Elsevier; 2022.
36. Meyer F, Crawford N. Optimizing process conditions and ensuring end product requirements of plastics with rheological analysis. Application Note AN52341 2018.
37. Ajinjeru C, Kishore V, Liu P, et al. Determination of melt processing conditions for high performance amorphous thermoplastics for large format additive manufacturing. *Addit Manuf*. 2018;21:125-132.
38. Albano C, Sanchez G. Study of the mechanical, thermal, and thermodegradative properties of virgin PP with recycled and non-recycled HDPE. *Polym Eng Sci*. 1999;39(8):1456-1462.
39. Larsen ÅG, Olafsen K, Alcock B. Determining the PE fraction in recycled PP. *Polym Test*. 2021;96:107058.
40. Bashirgonbadi A, Ureel Y, Delva L, Fiorio R, van Geem KM, Ragaert K. Accurate determination of polyethylene (PE) and polypropylene (PP) content in polyolefin blends using machine learning-assisted differential scanning calorimetry (DSC) analysis. *Polym Test*. 2024;131:108353.
41. Gaur U, Wunderlich B. Heat capacity and other thermodynamic properties of linear macromolecules. II. Polyethylene. *J Phys Chem Ref Data*. 1981;10(1):119-152.
42. Xu F, Wang B, Yang D, Hao J, Qiao Y, Tian Y. Thermal degradation of typical plastics under high heating rate conditions by TG-FTIR: pyrolysis behaviors and kinetic analysis. *Energy Convers Manag*. 2018;171:1106-1115.
43. Dai L, Zhou N, Lv Y, et al. Pyrolysis technology for plastic waste recycling: a state-of-the-art review. *Prog Energy Combust Sci*. 2022;93:101021.
44. Aboulkas A, El Bouadili A. Thermal degradation behaviors of polyethylene and polypropylene. Part I: pyrolysis kinetics and mechanisms. *Energy Convers Manag*. 2010;51(7):1363-1369.
45. Islam M, Trevorah RM, Appadoo DRT, Best SP, Chantler CT. Methods and methodology for FTIR spectral correction of channel spectra and uncertainty, applied to ferrocene. *Spectrochim Acta A Mol Biomol Spectrosc*. 2017;177:86-92.
46. ASTM. D7399-18: Standard Test Method for Determination of the Amount of Polypropylene in Polypropylene/Low Density Polyethylene Mixtures Using Infrared Spectrophotometry. 2018.
47. Higgins F. *Determination of Percent Polyethylene in Polyethylene/Polypropylene Blends Using Cast Film FTIR Techniques*. Agilent Technologies; 2012.
48. Camacho W, Karlsson S. NIR, DSC, and FTIR as quantitative methods for compositional analysis of blends of polymers obtained from recycled mixed plastic waste. *Polym Eng Sci*. 2001;41(9):1626-1635.
49. Xiao C, Ernst C. Analyzing Recycled Polyethylene Resin for Polypropylene Contamination Using FT-IR. 2014.
50. Vervoort S, den Doelder J, Tocha E, et al. Compatibilization of polypropylene–polyethylene blends. *Polym Eng Sci*. 2018;58(4):460-465.
51. Pfaendner R. Restabilization–30 years of research for quality improvement of recycled plastics review. *Polym Degrad Stab*. 2022;203:110082.
52. Winter H, Fritz H. Design of dies for the extrusion of sheets and annular parisons: the distribution problem. *Polym Eng Sci*. 1986;26(8):543-553.
53. Masato D, Kazmer D, Gruber A. Meta-analysis of thermal contact resistance in injection molding: a comprehensive literature review and multivariate modeling. *Polym Eng Sci*. 2023;63(12):3923-3937.

SUPPORTING INFORMATION

Additional supporting information can be found online in the Supporting Information section at the end of this article.

How to cite this article: Kazmer DO, Nzeh SO, Shen B, et al. Characterization, processing, and modeling of industrial recycled polyolefins. *Polym Eng Sci*. 2024;64(10):4801-4815. doi:10.1002/pen.26882